JTTEE5 12:214-225

HVOF Thermal Spray Deposited Y_2O_3-Stabilized ZrO_2 Coatings for Thermal Barrier Applications

Tabbetha A. Dobbins, Richard Knight, and Merrilea J. Mayo

(Submitted 6 August 2001; in revised form 3 March 2002)

High velocity oxy-fuel (HVOF) thermal spray has been successfully used to deposit yttria-stabilized zirconia (YSZ) for thermal barrier coating (TBC) applications. Adherent coatings were obtained within a limited range of spray conditions using hydrogen as fuel gas. Spray parameters such as hydrogen-to-oxygen ratio, spray distance, and substrate cooling were investigated. Spray distance was found to have a pronounced effect on coating quality; adherent coatings were obtained for spray distances between 75 and 125 mm from the gun exit for the hydrogen-to-oxygen ratios explored. Compared to air plasma spray (APS) deposited YSZ coatings, the HVOF deposited coatings were more fully stabilized in the tetragonal phase, and of similar density, surface roughness, and cross-sectional microhardness. Notably, fracture surfaces of the HVOF coatings revealed a more homogeneous structure. Many theoretical models predict that it should not be possible to melt YSZ in an HVOF flame, and therefore it should not be possible to deposit viable YSZ coatings by this process. The experimental results in the present work clearly contradict those expectations. The present results can be explained by taking into account the effect of partial melting and sintering on particle cohesion, as follows. Combustion chamber pressures (P_o) of ~3.9 bar (58.8 psi) realized during HVOF gun operation allows adiabatic flame temperature values that are above the zirconia melting temperature. Under these conditions, the Ranz-Marshall heat transfer model predicts HVOF sprayed particle surface temperatures T_p that are high enough for partial melting of small (~10 μm) zirconia particles, $T_p = (1.10\text{-}0.95)T_m$. Further analysis shows that for larger particles (38 μm), adherent coatings are produced when the particle temperature, $T_p = 0.59\text{-}0.60\ T_m$, suggesting that sintering may have a role in zirconia particle deposition during HVOF spray. These results suggest two different bonding mechanisms for powders having a broad particle size distribution.

Keywords HVOF, TBC, zirconia

1. Introduction

Thermal barrier coatings (TBCs) are used to reduce the surface temperature of turbine components by as much as 140 °C.[1] In service environments where temperatures are in excess of 1300 °C, thermal barrier coatings potentially allow higher operating temperatures or longer component life. TBC lifetime and reliability, however, remain issues because thermal shock (due to thermal cycling) and oxidation of the underlying bond coat can lead to TBC spallation. Refurbishing these coatings using the current technology for TBC deposition, such as electron beam physical vapor deposition (EB-PVD) or air plasma spray (APS), is both costly and time-consuming. Coating restoration may be more convenient using high velocity oxy-fuel (HVOF) thermal spray because of its simpler operational design, requiring neither a high vacuum, as in EB-PVD, nor a high voltage (40-80 kW direct current) power supply as in APS deposition.

HVOF thermal spray technology has attracted increased attention recently because of its ability to deposit highly dense coatings of low melting temperature composite and alloy powders such as WC-Co,[2] Cr_3C_2-NiCr,[2] TiC-Ni,[3] Inconel 718,[2,4] Inconel 625,[2,4] and copper-nickel-indium alloys.[2] The potential for using HVOF combustion spray to deposit yttria-stabilized zirconia (YSZ) coatings for thermal barrier (TBC) applications has largely been ignored because HVOF has a much lower deposition temperature that may preclude complete melting of the YSZ particles in the flame. Traditionally, APS had been used for depositing YSZ for TBC applications because the plasma source yields jet temperatures as high as ~14 000 K, generally ensuring complete particle melting during deposition. A conventional requirement for the deposition of viable coatings by thermal spray techniques is complete particle melting during deposition.

In practice, the adiabatic flame temperature in the HVOF combustion chamber depends on the fuel gas used, fuel-to-oxygen ratio, gas flow rates, and combustion chamber pressure. The highest flame temperatures reportedly attained in the HVOF system are 3,160 °C using acetylene fuel gas[5] and 2896 and 2856 °C using propylene and hydrogen, respectively.[5] However, the cooling necessary to maintain the structural integrity of the copper gun nozzle removes an estimated 5-25 kW h of heat from the flame, leaving even less energy for heating the YSZ particles. YSZ is a high melting temperature refractory ceramic having a melting temperature of 2,677 °C. Moreover, the low

Tabbetha A. Dobbins, Department of Materials Science and Engineering, The Pennsylvania State University, University Park, PA 16802 (presently at 100 Bureau Drive, Stop 8520, Gaithersburg, MD 20899-8520); **Richard Knight,** Center for the Plasma Processing of Materials, Department of Materials Engineering, Drexel University, 32nd and Chestnut Sts., Philadelphia, PA 19104; and **Merrilea J. Mayo,** Department of Materials Science and Engineering, The Pennsylvania State University, University Park, PA 16802 (presently at GUIRR, Room 510, The National Academies, 500 5th St. NW, Washington, DC 20001). Contact e-mail: tabbetha.dobbins@nist.gov.

thermal conductivity (~1.1W/m/K) of zirconia could introduce problems with intra-particle heat conduction and melting at the core of the 40 μm diameter particles typically used for thermal spray deposition processes.[6]

Several authors have modeled the in-flight melting and impact behavior of ceramic particles in an HVOF jet.[3,6,7] Joshi constructed a finite difference model of particle heat-up and acceleration, which includes Knudsen non-continuum effects.[3,6] According to the Joshi model, the Knudsen non-continuum effect will have a large impact on the jet to particle heat transfer for particle sizes below 50 μm in an HVOF flame.[3,6] Joshi calculated the core temperature of alumina and zirconia particles in an HVOF flame. The model predicted that unmolten zirconia remains at the particle core for zirconia particles as small as 10 μm.[3,6] This modeling work makes the HVOF deposition of molten zirconia seemingly impossible.[3,6]

A few models suggest that complete particle melting is not absolutely required in order for successful zirconia coating deposition by HVOF to occur. Kadyrov et al. included the effect of heat generated by particle collision with the substrate into calculations to determine zirconia particle melting behavior during HVOF deposition.[7] It was shown that a 10 μm diameter zirconia particle accelerated in a supersonic jet reached a 94% molten state if all of the particle's kinetic energy is transformed into heat, which then is re-absorbed by the particle upon impact.[7] Kadyrov et al. arrived at this solution employing a stoichiometric, hydrogen fueled flame having a reported temperature of 2727 °C (at 9.7 bar or 145 psi). This modeling work demonstrated the possibility that the HVOF flame could melt YSZ and other high melting temperature powders.

It has been experimentally shown that the high velocity of the flame generates large-scale eddies and vortices,[8] which small (~5 μm) particles would follow, leading to segregation to the jet periphery where they would not experience the maximum flame temperatures.[8] However, recent work on the HVOF deposition of nanocrystalline Inconel 718 having a slightly larger mean particle size of 10 μm[9] and alumina having an average particle size of 15 μm[10,11] suggested that particles as small as 10 μm particles will travel along the center-line of the HVOF jet. Ramm et al. and Sturgeon et al. deposited alumina coatings by HVOF using starting powders having a mean particle size of 15 μm.[10,11] These coatings compared well with alumina coatings deposited by air plasma spray.[11] The results also expose a discrepancy between earlier predictions and actual particle deposition behavior during HVOF spraying[10,11] in that small particle sizes may be required for complete melting of high temperature refractory materials during HVOF spray, but they may not be required to be as small as 5 or 10 μm in order for deposition to occur. As additional evidence that HVOF is capable of depositing high melting temperature particles, TWI in the UK issued a very brief report in 1995 that the researchers were able to use HVOF spray to deposit YSZ; however, no further discussion of adhesion, microstructure or overall coating quality was given for these coatings.[12] The work of Cole et al. is the earliest work clearly demonstrating the ability of HVOF to deposit YSZ coatings.[13] However, the highly ignitable acetylene fuel gas, used in this study because of its high combustion temperature, permitted only low gas pressures (1.47 bar or 22 psi) to be used. Modifications to the gas supply in the HVOF gun designed were required to deliver the acetylene gas without further pressure drop and allow the gun to operate at conditions approaching supersonic.[13] In summary, there is no consensus that high melting temperature refractories can be deposited by conventional, supersonic HVOF guns, and no clear evidence that YSZ can be deposited, in particular. The present work, therefore, attempts to answer some open questions surrounding YSZ deposition by HVOF.

List of Symbols

P_o	combustion chamber stagnation pressure, bar
d_{50}	mean particle diameter, μm
R_a	surface roughness average, μm
Φ	flame equivalence ratio
M_j	Mach number
U	jet velocity, m/s
U_j	maximum jet velocity, m/s
α	exponential decay constant for jet velocity
X	axial distance, m
X_c	potential core length, m
D	nozzle diameter, mm
T	jet temperature, °C
T_j	maximum jet temperature, °C
T_a	ambient temperature, °C
T_p	particle surface temperature, °C
T_p^o	initial particle surface temperature, °C
T_m	zirconia melting temperature, °C
V_p	particle velocity, m/s
V_p^o	initial particle velocity, m/s
ρ_s	zirconia particle density, g/cm^3
d_p	particle diameter, μm
η_g	integral mean gas viscosity, N s/m^2
ρ_g	integral mean gas density, g/cm^3
κ_g	integral mean gas thermal conductivity, W/m K
C_d	coefficient of Drag
Re	Reynolds number
C_p	specific heat of zirconia, J/g K
h	Ranz-Marshall heat transfer coefficient, W/m^2 K
Nu	Nusselt number

2. Experimental Procedure

2.1 Materials

Tosoh Corporation (Belle Meade, NJ) manufactured the 5.4 wt.% YSZ starting powder used for HVOF deposition. The composition of the YSZ starting powder is listed in Table 1. The yttria content of the starting powder used for these experiments was slightly lower than the 6-8 wt.% considered optimum for thermal barrier coating applications.[14] However, the slightly lower yttria content powder used for these experiments has no significant effect on the melting temperature of the particles.[15] The mean particle size (d_{50}) by volume, determined using a Malvern Mastersizer S (Southborough, MA) particle size analyzer, was 38 μm. The 38 μm particles were spray-dried granules comprised of smaller, ~200 nm agglomerates, comprised in turn of 27 nm crystallites (crystallite sizes reported by the Tosoh Corp.). The crystallite size in the starting powders was also determined

in the present work by x-ray diffraction (XRD) line broadening. The results yielded slightly larger crystallite size (40.6 nm) than was reported by the manufacturer. A micrograph of the starting powder is shown in Fig. 1. For HVOF studies, 25 × 25 × 7.5mm nickel-based superalloy substrate test pieces were first coated on one side with a 150 μm thick Ni-22Cr-10Al-1Y bond coat by APS at the Engelhard Corporation (East Windsor, CT).

2.2 Thermal Spray Deposition

The YSZ powder was deposited using a Stellite Coatings Inc. Jet-Kote II-A system (Goshen, IN) with a 153.8 mm long and 6.35 mm inner diameter nozzle at Drexel University's Center for Plasma Processing of Materials (DU-CPPM, Philadelphia, PA). The total combustion chamber pressure (P_o) used during these experiments was 3.9 bar (58.8 psi). Hydrogen-rich flames having oxygen-to-fuel ratios of 0.385, 0.420, and 0.463 were used during these experiments. The powders were hopper fed using a Plasmadyne (Santa Anna, CA) volumetric powder feeder with an argon carrier gas. The substrates were fixed on a stationary support and the HVOF gun was mounted onto a Sulzer Metco (Westbury, NY) X-Y traverse fixed at standoff distances of 75, 100, and 125 mm. The gun moved horizontally across the substrate right-to-left or left-to-right. Multiple (~4) traverses, each offset from the next, were required to cover the entire substrate area. A single pass was achieved only when the entire substrate had been traversed in this manner. The 150-300 μm thick coatings were typically deposited in 4 or 5 passes. In some cases, chilled water (25 °C) provided substrate cooling via a copper chill-block located behind the substrate. In all cases, substrate pre-heats were performed in an initial gun pass without YSZ powder. Spray parameters for the HVOF coatings are given in Table 2.

Air plasma sprayed YSZ coatings were deposited by the Engelhard Corporation and used for comparison with the HVOF coatings.

2.3 Characterization Techniques

The HVOF and APS deposited YSZ coatings were vacuum infiltration epoxy mounted and the mounts were cut in cross-section. The metallographic cross sections were polished to a 1-μm diamond finish and examined by scanning electron microscopy. The fracture surfaces of both coating types were prepared and examined by scanning electron microscopy. Pore volume was determined by the point count method[16] using 500× micrographs. The porosity mean and deviation reported are the result of measurements taken from six different HVOF coatings.

The surface roughness of the YSZ coatings was measured using a Tencor Instruments Alpha-Step 200 stylus tracing profilometer (Milpitas, CA). The stylus tip scanned a distance of 2000 μm on the sample surface at a scan rate of 250 μm/s. The roughness (R_a) reported was the mean of four values scanned from different areas on a YSZ coating surface. The roughness of the Ni-22Cr-10Al-1Y bond coat layer was measured as well. The same bond coats were used for both the APS and HVOF deposited YSZ samples. The bond coats were deposited at the Engelhard Corporation.

Vickers microhardness values were measured on polished crosssections using a Leco V-100-C1 hardness tester (St. Joseph, MI). Indentations were made in the coatings using a 0.3 kg load for 5 s. The reported microhardness values are the average of six samples in which ten indentations were made at random locations along the sample cross-section. The microhardness of sintered compacts of known density were measured for comparison. The sintered compacts were prepared using the commercial Tosoh Corp. YSZ powder. The density of the sintered compacts was determined by the Archimedes' immersion technique using water as the medium. Microhardness values reported for the sintered compacts are an average of six indentations made at random locations on the compact surface.

XRD was performed on the both APS and HVOF deposited YSZ coatings to determine the crystalline phases present. A Rigaku Geigerflex x-ray diffractometer (Wakefield, MA) was used. XRD line broadening (XRDLB) of the (111) tetragonal peak located at 30.168° was used to determine the crystallite size in the coatings in the manner of the Scherrer technique.[17]

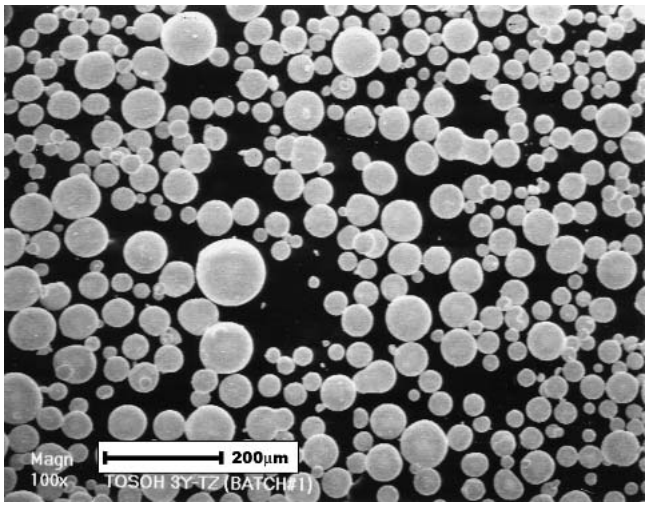

Fig. 1 The Y_2O_3-stabilized ZrO_2 starting powder used for HVOF deposition is a commercial powder manufactured by the Tosoh Corp. The composition of the starting powder is listed in Table 1.

Table 1 Chemical Composition of the Yttria-Stabilized Zirconia Powders Used for HVOF Thermal Spray Manufactured by Tosoh Corporation (a)

Chemical Compound	Composition of Powder, wt.%
ZrO_2	balance
Y_2O_3	5.15
Al_2O_3	<0.005
SiO_2	0.006
Fe_2O_3	0.003
Na_2O	0.021

(a) Chemical analysis provided by Tosoh Corporation

3. Results and Discussion

3.1 Particle and Gas Dynamics

3.1.1 Effect of Hydrogen-to-Oxygen Ratio. The adiabatic flame temperature was calculated for a range of flame stoichi-

Table 2 Spray Parameters Used to Investigate HVOF Thermal Spray Deposition of YSZ

Sample No.	Equivalence Ratio Φ	Combustion Pressure, Bar	Total Gas Flow Rate, kg/s	Spray Distance, mm	Chilled Water Temperature
1	1.29	4.1	0.005944	100	none
2	1.29	4.1	0.005944	100	25 °C
3	1.29	4.1	0.005944	75	none
4	1.29	4.1	0.005944	125	none
5	1.18	3.97	0.005874	100	none
6	1.18	3.97	0.005874	100	25 °C
7	1.18	3.97	0.005874	75	none
8	1.07	3.81	0.005804	100	none

ometries using the Chem-Sage thermochemical equilibrium modeling software developed by GTT Technologies (Aachen, Germany). The Chem-Sage thermochemical equilibrium calculations were performed considering the equilibrium reaction

$$H_2 + \frac{0.5}{\Phi} O_2 \rightarrow aH_2O + bOH + cH + dO + eO_3 + fH_2O_2 + gHO_2 + hH_2 + iO_2 \quad \text{(Eq 1)}$$

where Φ is an expression of the hydrogen-to-oxygen ratio called the equivalence ratio, defined as

$$\Phi = \frac{H_2}{O_2} \Big/ \left(\frac{H_2}{O_2}\right)_{\text{stoichiometric}} \quad \text{(Eq 2)}$$

and a-i are the equilibrium amounts of the gaseous species. Most computational models for HVOF gas dynamics assume an equilibrium reaction in the combustion chamber although the reaction does not proceed to yield equilibrium products during actual HVOF gun operation.[18] The equivalence ratios (Φ) used in this work were 1.29, 1.18, and 1.07, corresponding to adiabatic flame temperatures of 2965, 2983, and 2989 °C, respectively.

3.1.2 Effect of Combustion Chamber Pressure. Adiabatic combustion flame temperatures are typically reported for 0.98 bar of total pressure. Chem-Sage thermochemical calculation software allows the adiabatic flame temperature to be calculated for various pressures. Figure 2 shows the isobaric variation in adiabatic flame temperature with equivalence ratio (Φ). The combustion chamber pressures used in Figure 2 are 0.98, 3.9, 7.8, and 9.8 bar. In the present study, combustion chamber pressures were calculated using the Jet-Kote II gun geometry and gas flow rates assuming adiabatic, isentropic fluid flow within the gun nozzle. These assumptions are valid provided that the gun nozzle walls are smooth, so that frictional effects can be neglected, and the gas has zero viscosity, eliminating irreversible effects on fluid flow.[19] Results show the HVOF deposition experiments were performed using a combustion pressure (P_o) of ~3.9 bar (Table 2). As can be seen in Fig. 2, the adiabatic flame temperature varies by as much as 300 °C with variations in total gas pressure in the combustion chamber. Using 3.9 bar total pressure, flame stoichiometries having equivalence ratios between ~0.35 and ~2.2 have adiabatic temperatures higher than the melting temperature of YSZ.

3.1.3 HVOF Flame Temperature and Velocity Profiles. Tawfik et al. developed a set of empirical generalized equations for the gas velocity and temperature in an HVOF flame.[20] The equations are valid for Mach numbers (M_j) between 1.5 and 2.5. The generalized equations were tested experimentally for consistency with gas dynamics using a Hobart Tafa JP-5000 HVOF gun fueled with kerosene gas.[20] The generalized equation for flame velocity is

$$\frac{U}{U_j} = 1 - \exp\left(\frac{\alpha}{1 - X/X_c}\right) \quad \text{(Eq 3)}$$

where U is the gas velocity, U_j is the maximum gas velocity, α is the exponential decay constant taken as 0.85 (20), X is the axial distance along the gun barrel, and X_c is the potential core length. The potential core is the supersonic region containing the shock-diamond structure,[8,20] and its length (X_c) is a function of nozzle diameter (D) and jet Mach number (M_j):

$$\frac{X_c}{D} = 3.5 + 1.0M_j^2 \quad \text{(Eq 4)}$$

Physically, both the potential core length (X_c) and the exponential decay constant are also related to the flame density ratio between jet and ambient conditions.[22] The exponential decay constant, α, has a dependence on jet Mach number, as well.[22] The nozzle diameter (D) of the Stellite Coatings (Goshen, IN) Jet Kote II gun is 6.35 mm. The jet Mach number is M_j = 1.97 as mentioned above. The maximum gas velocity (U_j) was taken as 2690 m/s due to the jet Mach number (M_j) of 1.97, calculated at the exit plane for the conditions of gas flow used in this study.

The generalized flame equations from this prior work were applied in the present work to yield flame velocity and temperature profiles for an HVOF H_2-O_2 combustion flame without further modification. However, comparison between the generalized flame equation values and available hydrogen flame velocity data show that the standard deviation in potential core length and exponential decay constant are 0.6 mm and 0.8 a.u., respectively.[21] Figure 3(a) shows graphically the flame velocity along the gun axis using the generalized flame velocity equation. In this case, the potential core length X_c is 50.8 mm. The calculated potential core length shows good agreement with the 40-50 mm potential core lengths measured on subsonic hydrogen flames by laser Doppler velocimetry.[21] This agreement indicates that potential core length does not vary substantially with Mach number. Prior velocity measurements for hydrogen flames have shown larger values of the exponential decay constant ($\alpha \cong 2$). However, the velocity measurements were performed on flames traveling at subsonic velocities[21] and so direct correlation with α is not expected. The exponential decay constant α determined for use in the generalized flame equa-

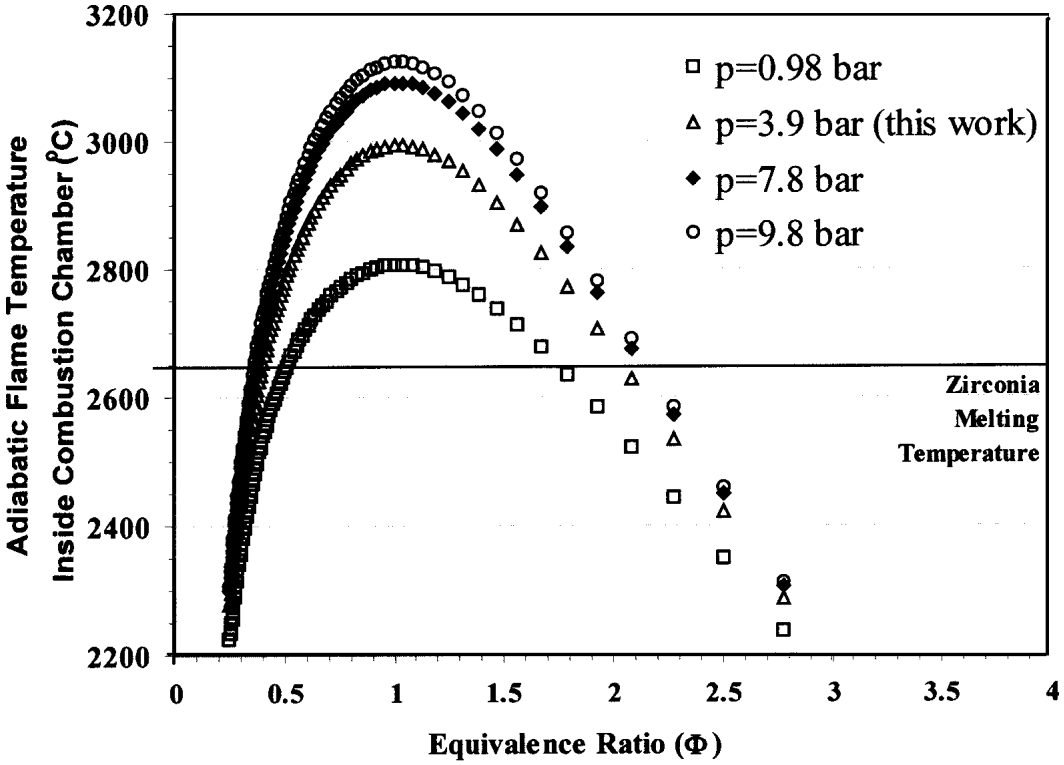

Fig. 2 Adiabatic flame temperature of H_2-O_2 flames under various pressures. The combustion chamber pressure used for this work was 3.9 bar (△). Other combustion chamber pressures considered in these calculations were 9.8 bar (○), 7.8 bar (◆), and 0.98 bar (□). The data were generated using Chem-Sage thermochemical calculation software.

tion[20] was developed for a HVOF gun system and is, therefore, more closely related to this study.

Figure 3(b) shows the generalized equation for flame temperature profile from the equation:

$$\frac{T - T_a}{T_j - T_a} = 1 - \exp\left(\frac{1.25}{1 - X/X_c}\right) \quad \text{(Eq 5)}$$

where T_a is ambient temperature (25 °C) and T_j the maximum jet temperature. The maximum jet temperatures (T_j) used in the equation was 2965 °C, the adiabatic flame temperature for Φ = 1.29 and P_o = 3.9 bar, without consideration for the cooling imparted by the copper gun nozzle.

3.1.4 HVOF Particle Temperature and Velocity Profiles. Certain combinations of experimental parameters enabled adherent YSZ coatings to be produced by HVOF. Spray conditions successful in yielding adherent coatings were hydrogen-to-oxygen equivalence ratios (Φ) of 1.29, 1.18, and 1.07, and spray distances of less than 125 ± 5 mm. Analytical solutions to the momentum and heat transfer equations were implemented to determine the particle velocity and temperature during deposition.[23] The analytical solution to the momentum transfer equation ignores gravitational, Basset history, or centrifugal forces acting on the particle. The momentum transfer equation is numerically solved

$$V_p = U - (U - V_p^o)\exp\left(\frac{-\partial t}{\tau}\right) \quad \text{(Eq 6)}$$

where V_p, U, and V_p^o are particle velocity, jet velocity, and initial particle velocity, respectively. The variable τ is expressed by the following

$$\tau = \frac{24\rho_s d_p^2}{18\eta_g C_d \mathrm{Re}} \quad \text{(Eq 7)}$$

where ρ_s is the zirconia particle density (6.08 g/cc), d_p is particle diameter, η_g is the integral mean gas viscosity, C_d is the coefficient of drag, and Re is the Reynolds number. The coefficient of drag for spherical particles as a function of the Reynolds number[23] is described as follows:

$$C_d = \frac{24}{\mathrm{Re}}(1 + 1.015\mathrm{Re}^{0.687}) \quad \mathrm{Re} \le 1000$$
$$C_d = 0.44 \quad \mathrm{Re} > 1000 \quad \text{(Eq 8)}$$

The particle Reynolds number is calculated by the following:

$$\mathrm{Re} = \eta_g \frac{(|V_g - V_p|)}{\rho_g} d_p \quad \text{(Eq 9)}$$

where ρ_g is the integral mean gas density.

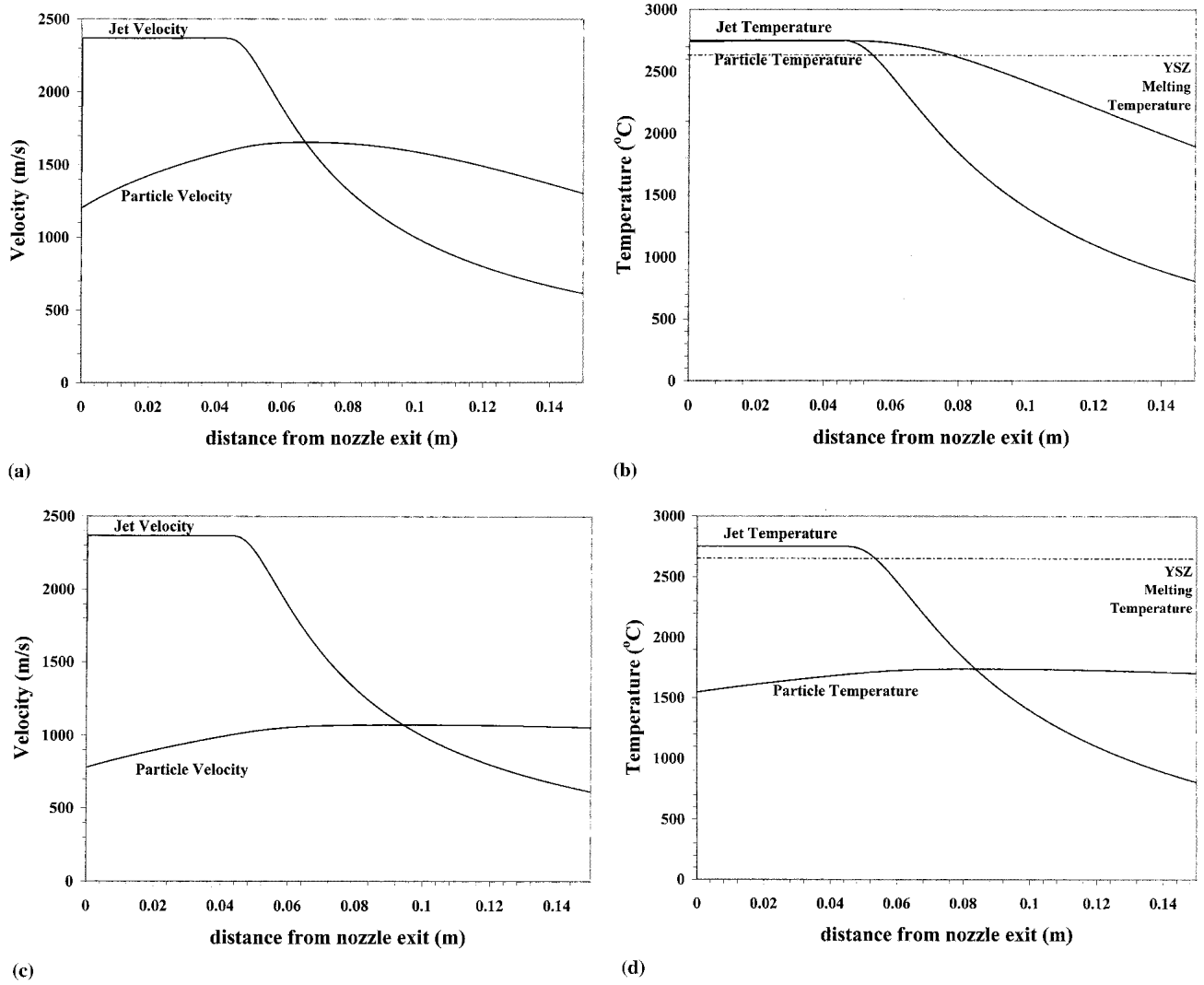

Fig. 3 Tawfik et al.[15] generalized equations for HVOF jet velocityand temperature. The potential core length (X_c) is the supersonic region containing the shock-diamond structure.[8] This constant velocity region is followed by an exponential decay velocity function. The exit flame velocity at the nozzle exit is 2686 m/s and the particle injection velocity is 20 m/s. **(a)** The flame and particle velocity profiles for a 10 μm YSZ particle. **(b)** The flame and particle temperature profiles for a 10 μm YSZ particle. The maximum flame temperatures correspond to the adiabatic flame temperatures for one of the three flames used in this work, namely Φ = 1.29. Coatings were deposited for 75-125 mm spray distances. The temperature of a 10 μm particle at these distances is near the melting point of YSZ: T_p= (1.10-0.95)T_m. **(c)** The flame and particle velocity profiles for a 38 μm YSZ particle. **(d)** The flame and particle temperature profiles for a 38 μm YSZ particle. The maximum flame temperature is 2965 °C. Since coatings were deposited for 75-125 mm spray distances, the temperature of a 38 μm particle during deposition is T_p = (0.59-0.60)T_m.

The Ranz-Marshall heat transfer equation was used to determine particle temperature,

$$T_p = T_g - (T_g - T_p^o)\exp\left(\frac{-6h\partial t}{\rho_s c_p d_p}\right) \quad \text{(Eq 10)}$$

where T_p, T_g, and T_p^o are particle temperature, gas temperature, and initial particle temperature, respectively, c_p is specific heat of the zirconia particle (604J/kg K), and h is the heat transfer coefficent. The expression for the heat transfer coefficient h is

$$h = \frac{\mathrm{Nu} \cdot k_g}{d_p} \quad \text{(Eq 11)}$$

where Nu is the Nusselt number and k_g is the integral mean gas thermal conductivity. The details of the numerical formulation to solve the momentum and heat transfer are described elsewhere.[23]

Figure 3(a) shows the gas and particle velocity trajectories after exit from a 150 mm nozzle. The particle injection velocity used in the model is 20 m/s. Figure 3(b) shows that 10 μm zirconia particles will realize temperatures above the melting temperature from the exit to a spray distance of 90 mm. Experimentally, coatings were obtained for spray distances between 75 and 125 mm. A 10 μm particle thus experiences temperatures ranging from 1.10-0.95 T_m, suggesting that partial melting of these particles occurs during successful deposition. Figures 3(c) and 3(d) show the particle temperature and velocity profile outside of the gun nozzle for 38 μm particles, the mean particle size in

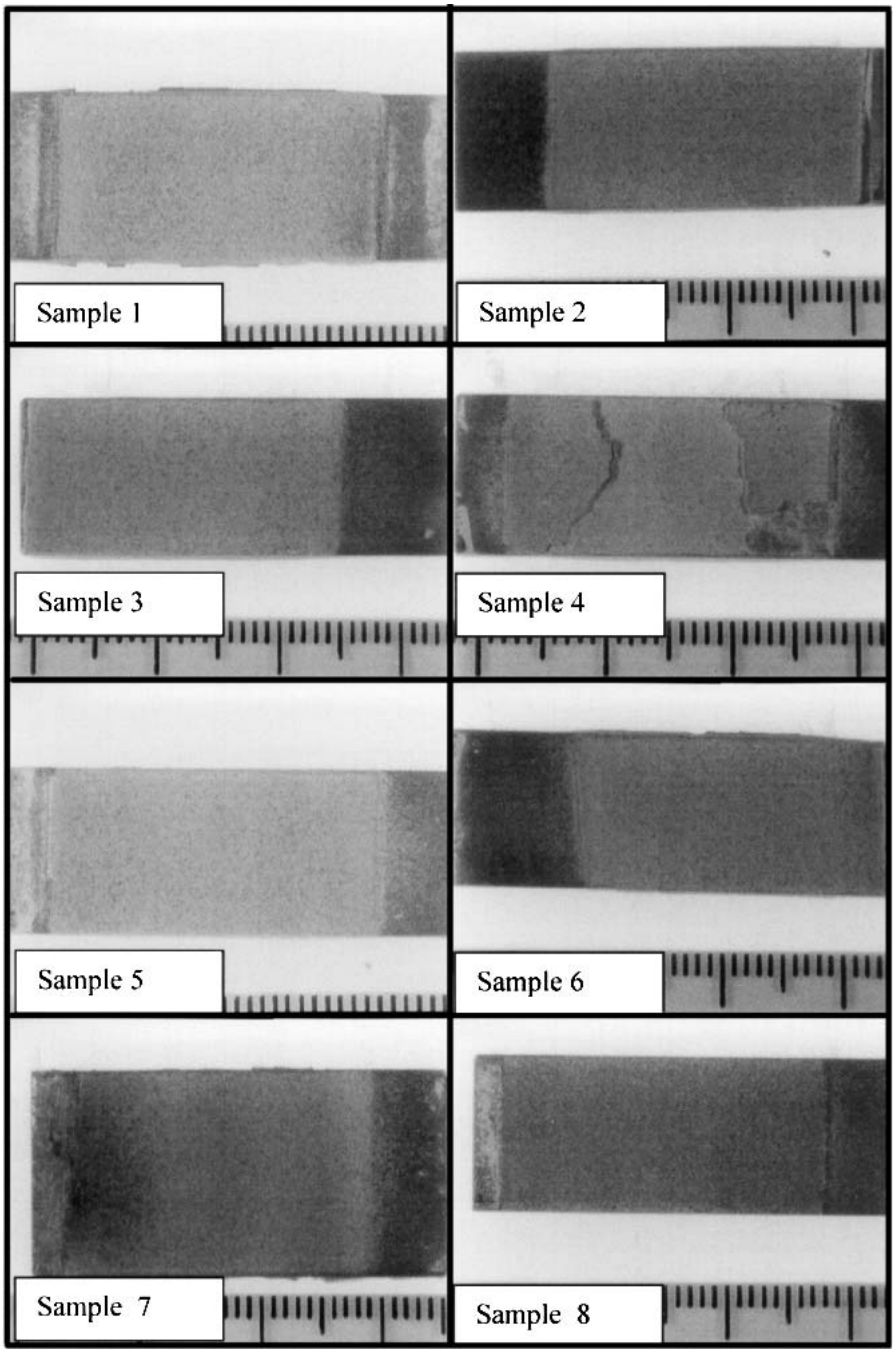

Fig. 4 HVOF coated test pieces 1-8. Corresponding spray parameters are listed in Table 2. Spray parameters that yielded adherent coatings[1-3,5-8] were flame compositions having equivalence ratios (Φ) of 1.29, 1.18, and 1.07 and spray distances of 75 and 100 mm. Sample 4 was deposited using a spray distance of 125 mm using an equivalence ratio of 1.29.

the present powder. For 38 μm, the particle temperature during successful deposition is 0.59-0.60 of T_m, suggesting that the inter-particle cohesion mechanism for larger particles is more related to sintering than melting.

3.2 Properties of HVOF and APS Thermal Spray YSZ Coatings

3.2.1 HVOF vs Air Plasma Spray Deposited YSZ Coating Microstructures. Figure 4 shows photographs of several HVOF deposited samples (no. 1-8) corresponding to the deposition conditions given in Table 2. Test pieces that experienced peeling (e.g., sample no. 4) were also subjected to metallographic examination. The microstructures of YSZ coatings deposited by high velocity oxy-fuel (HVOF) and air plasma spray (APS) are shown in Fig. 5. The thickness of the HVOF deposited YSZ coatings were on average 250 μm, obtained in 5-10 gun passes. The HVOF spray deposited YSZ coatings are characterized by vertical cracks and fine scale interlamellar porosity. The

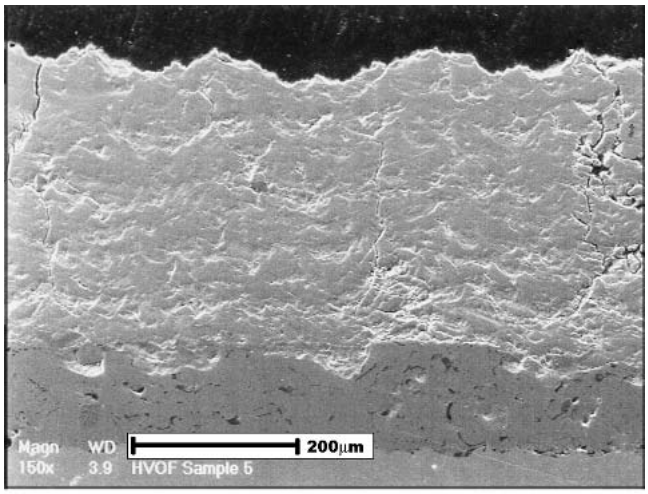

(a)

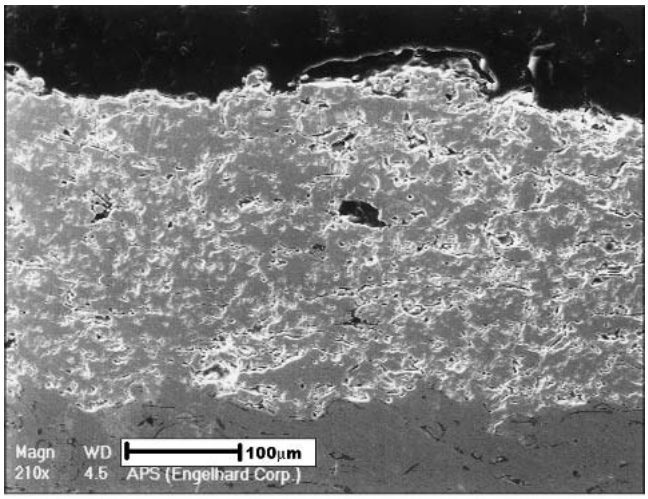

(b)

Fig. 5 Polished cross sections of Y_2O_3-stabilized ZrO_2 (YSZ) coatings deposited by **(a)** high velocity oxy-fuel (HVOF) and **(b)** air plasma spray (APS). (a) HVOF deposited Y_2O_3-stabilized ZrO_2 coating (Conditions: $\Phi = 1.07$, spray distance = 100mm without chilled water cooling). The HVOF deposited coatings contained 21 ± 6.3 vol% porosity by the point count method. Micrograph is taken at 150×. (b) APS deposited Y_2O_3-stabilized ZrO_2 coating contains 26 ± 4.3 vol% porosity by the point count method. Micrograph is taken at 210×.

vertical cracks may be attributed, in part, to highly dense regions within the coatings, which yield a higher modulus and hence high internal stresses for a fixed strain. Both the HVOF and the APS deposited YSZ coatings have morphologies containing interlamellar pores, which are consistent with the splat microstructures of thermal spray coating. However, the interlamellar porosity in the HVOF coatings appears much finer, and single crystallites bridging across splat boundary regions are seen in Fig. 6, whereas the APS deposited coatings contain large, round pores not seen in the HVOF coatings. Single crystallites bridging across porosity are not observed in APS deposited coatings; rather the large pores in the APS coatings are bordered on all sides by non-bridging crystallites. The single crystallite bridges observed in HVOF coatings may indicate the occurrence of

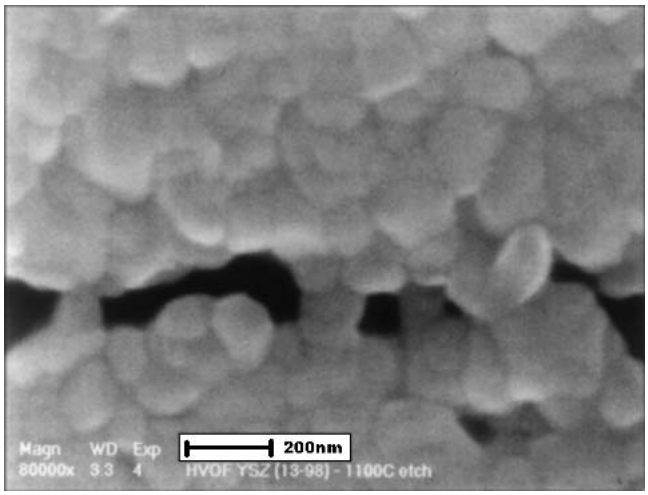

Fig. 6 Micrograph shows single crystallites bridging across an interlamellar pore in the HVOF coating. These bridging crystallites are not observed in APS deposited coatings and could represent regions of solid-state sintering during HVOF deposition.

solid-state sintering during deposition. The volume of porosity in the HVOF and APS deposited coatings were 21 ± 6.3 and 26 ± 4.3 vol%, respectively, as determined by point count. The total pore volume of both YSZ coatings were within the range of standard deviation, and the difference was not considered significant.

The HVOF coatings have a more homogeneous grain size distribution than the APS coatings as shown qualitatively in Fig. 7. The nonuniform grain sizes in the APS coatings were attributed to grain coarsening due to heating by the plasma jet, which inputs significantly more heat during the multiple pass deposition process than the HVOF jet. The mean crystallite sizes in the HVOF and APS deposited coatings were 141 and 172 nm, respectively, as determined by XRDLB.

Cross-sectional views of the fracture surfaces of the two coatings are shown in Fig. 8. The APS fracture surface contained an intersplat, columnar structure indicating that directional solidification of impacted particles had occurred. The absence of this sort of directional solidification from the HVOF fracture surface indicates a lesser degree of melting. The finer, more homogeneous microstructure of the HVOF coatings may have some performance benefits, such as a more isotropic modulus, retention of the desirable tetragonal phase for longer times at high temperature, and fewer flaws to act as crack initiation sites leading to coating failure.

3.2.2. Surface Roughness of HVOF vs APS Deposited YSZ Coatings. The roughness average (R_a) of the bond coat was determined by stylus tracing profilometry to be 8.95 (±0.52) μm. The roughness averages (R_a) for the overlaying YSZ coatings are reported in Table 3. The values for the APS and HVOF deposited coatings are 10.13 (±1.40) μm and 13.10 (±1.61) μm, respectively. The surface roughness of the HVOF deposited YSZ coating falls within experimental error to that of the APS deposited YSZ coating. The similar surface roughness values found for the YSZ coatings are unexpected because typical APS deposited alumina coatings are reported to have a roughness average approximately three times that of HVOF deposited alu-

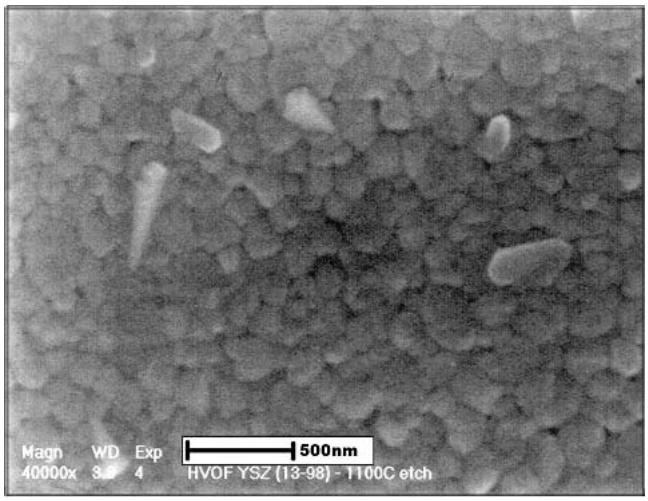

(a)

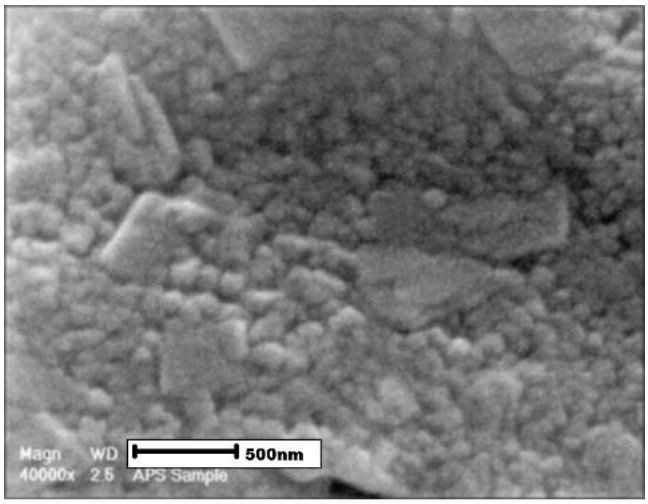

(b)

Fig. 7 Cross-sectional view of grain structures of YSZ coatings deposited by **(a)** HVOF and **(b)** APS at 40 000× magnifications. The HVOF deposited coating has a more uniform grain structure. (a) HVOF deposited YSZ coating has an average grain size of 141 nm as determined by XRDLB. (b) APS deposited YSZ coating has an average grain size of 172 nm as determined by XRDLB.

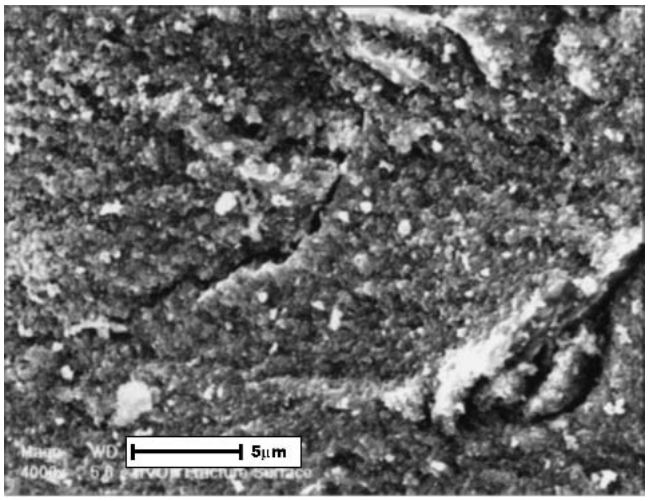

(a)

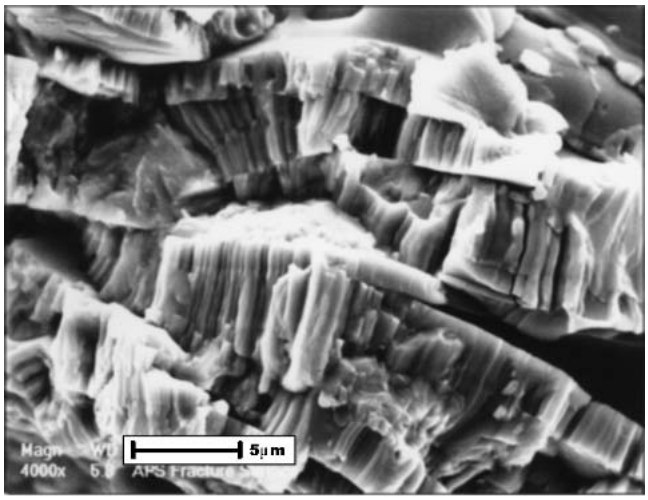

(b)

Fig. 8 Cross-sectional view of fracture surfaces of YSZ coatings deposited by **(a)** HVOF and **(b)** APS at 4000×. **(c)** The intrasplat columnar structure is absent from the HVOF deposited YSZ coating, which exhibits fine, equiaxed crystallites. **(d)** APS deposited YSZ coating fracture surface shows a columnar intrasplat structure indicative of directional solidification during splat quenching typical of air plasma spray deposited coatings.

mina coatings.[11] The lower surface roughness in the HVOF deposited alumina coatings, relative to APS deposited alumina, can be attributed to the higher impact velocity imparted during deposition and the ability of the HVOF gun to melt alumina. The HVOF deposited α-Al_2O_3 starting powders experienced 88% melting as indicated by the relative amounts of γ-Al_2O_3 and α-Al_2O_3 in the coatings.[11]

3.2.3 Microhardness of HVOF vs APS Deposited YSZ-Coatings. The Vickers microhardness values for the HVOF and APS YSZ coatings were 5.46 ± 0.56 GPa and 5.20 ± 0.69 Gpa, respectively. The differences in microhardness values for the HVOF and APS deposited YSZ coatings are not significant and are within the range of experimental error. The Vickers microhardness of plasma sprayed YSZ has previously been reported as 4.5 GPa for a coating containing 17.5 vol% porosity.[24] Figure 9 shows the relationship between Vickers microhardness and density for both the HVOF and APS deposited YSZ coating as well as sintered zirconia compacts of known density from this and previous work.[25] The plot clearly shows that the microhardness values of the sintered compacts and thermal spray deposited coatings follow an exponential trend in coating porosity as predicted by others.[25,26]

3.2.4 Phase Composition of HVOF vs APS Deposited YSZ Coatings. The XRD patterns of HVOF and APS coatings are shown in Fig. 10 along with the pattern for the feedstock powder. The monoclinic phase, although present in the feedstock powders used for HVOF deposition, was absent from the resulting coatings, suggesting that, in the present work, particle temperatures attained during thermal spraying were high enough to induce the monoclinic to tetragonal phase transition, which

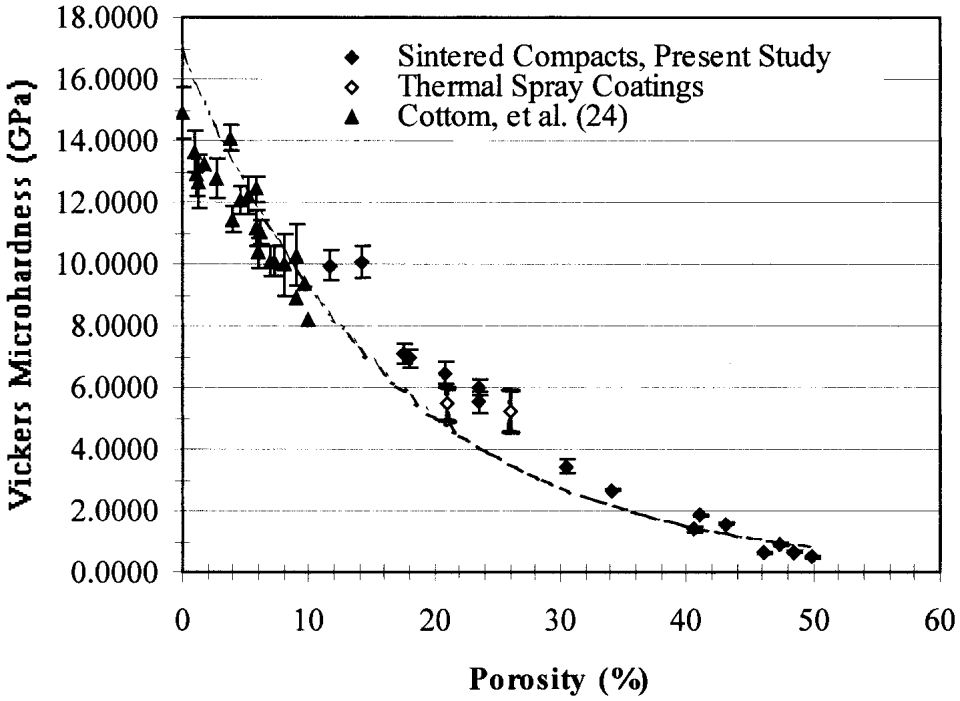

Fig. 9 Vickers microhardness as a function of density for sintered YSZ compacts (♦) prepared using the Tosoh Corp. TZ-3Y powders used later for HVOF deposition. The HVOF (5.46 ± 0.56 GPa) and APS (5.20 ± 0.69 GPa) deposited YSZ coatings (◇) used in this work are also represented. The data represented for lower than 10% porosity were taken from Ref. 24 (▲). The empirical curve-fit through the data, $H = 16.807e^{-0.06P}$ $R^2 = 0.95$, is representative of the microhardness dependence on porosity.

Table 3 APS and HVOF Spray YSZ Coating Properties

Deposition Process	Porosity, vol.%	Gain Size, nm	Surface Roughness, μm	Microhardness, GPa	Phase Constituents
HVOF	21 ± 6.3	141	13.1 ± 1.6	5.5 ± 0.56	*t*
APS	26 ± 4.3	172	10.1 ± 1.4	5.2 ± 0.69	t, minor m
APS NiCrAlY	…	…	8.95 ± 0.5	…	…

begins at ~590 °C and is complete at ~800 °C. Clearly, the tetragonal phase is dominant in the HVOF coatings. In comparison, a small amount of monoclinic phase was found in the APS coating, as shown in Fig. 10. A slow scan rate of 0.1 °/min from 72-76° was used to confirm the absence of the cubic phase from the starting powder and both coatings types. For both the HVOF and APS coatings, the diffraction patterns showed a small peak at 44°, which corresponds to the {111} peak of the underlying NiCrAlY bond coat.

The quenched-in tetragonal phase is common in air plasma spray thermal barrier coatings.[27-29] The monoclinic phase, however, is detrimental. More than 5 vol.% of the monoclinic phase means coating de-stabilization on cooling is possible, which would resulting in cracking and premature coating spallation. In general, air plasma spray coatings containing 0-1 vol.% of the monoclinic phase have higher resistance to thermal shock.[27] In the present study, a slow scan from 27-29° confirmed the presence of a small (<1 vol.%) amount of the monoclinic phase in the APS coatings deposited at Engelhard Corporation and did not reveal the presence of any monoclinic phase in the HVOF coating.

4. Conclusions

Yttria-stabilized zirconia coatings were deposited by HVOF within a narrow range of spray distances (75-125 mm) and several hydrogen-to-oxygen ratios having adiabatic flame temperatures above the YSZ melting temperature. The microstructure of the HVOF deposited YSZ coatings compared well with those deposited by APS. Porosity, microhardness, grain size, and phase constituents were very similar between the HVOF and APS YSZ coatings. Additionally, there may be some benefits offered by HVOF deposition of YSZ, including deposition of a finer and more homogeneous grain microstructure and creation of highly stabilized coatings.

The powders used for this study had a mean particle size of 38 μm and contained 2 vol.% 10-20 μm particles. Calculations of the adiabatic flame temperatures both within the HVOF spray nozzle and along the flame path indicate that the temperature of the HVOF jet using hydrogen fuel gas is high enough to at least partially melt small (~10 μm) zirconia particles. Using experimentally determined spray conditions deemed necessary to produce adherent coatings (i.e., spray distances of 75-125 mm), the

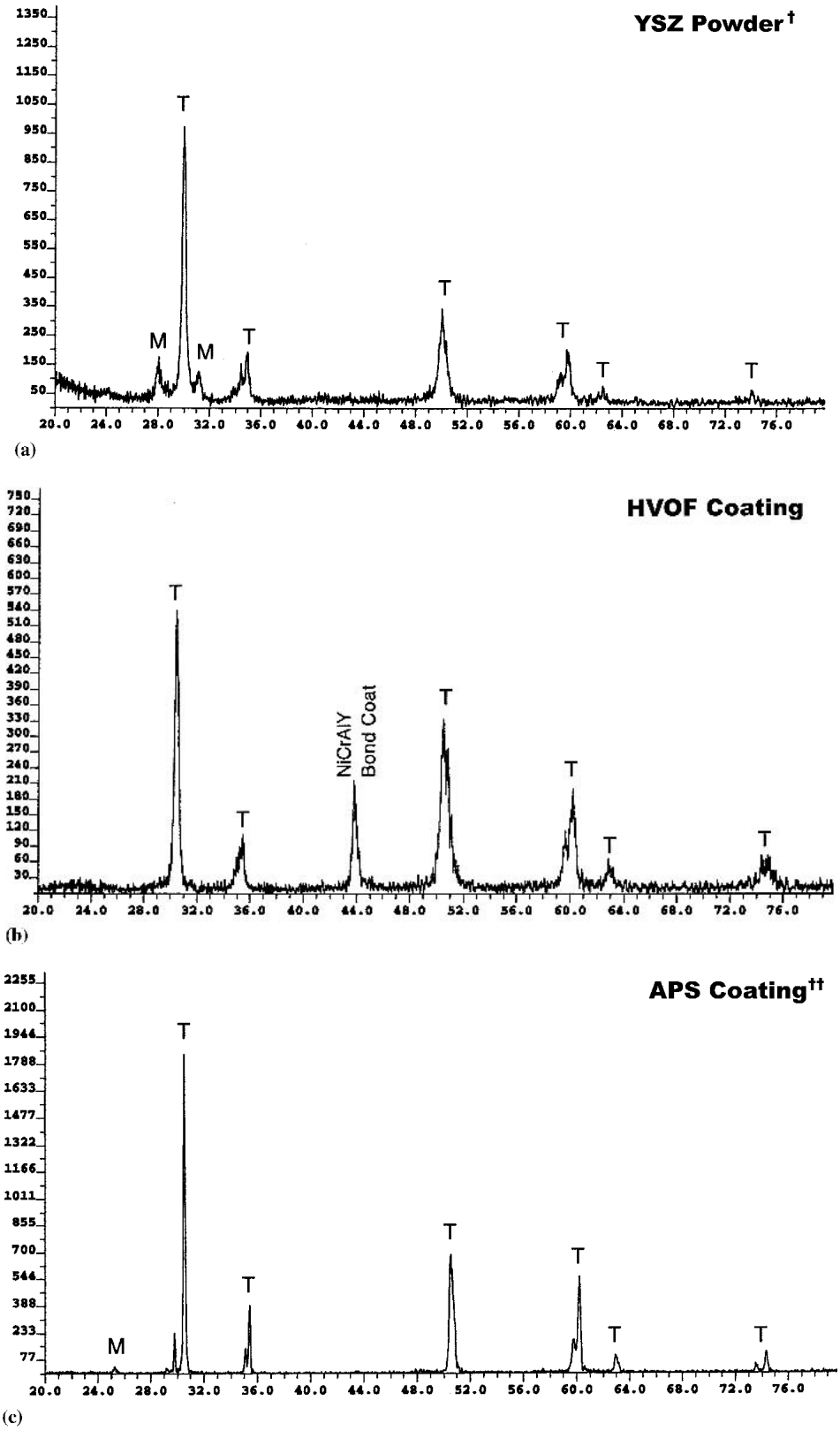

Fig. 10 XRD patterns for **(a)** starting powder, **(b)** HVOF coatings, and **(c)** APS coating.
(†) Commercial YSZ feedstock powder manufactured by the Tosoh Corp. was used this study. (††) Air plasma spray coating was deposited using a different YSZ feedstock powder.

particle temperatures required for the deposition of small (10 μm) and mean diameter (38 μm) particles were modeled. Mean diameter particles (~38 μm) experience temperatures only on the order of 0.59-0.60 T_m suggesting that, for these particles, sintering rather than melting may assist in particle cohesion during HVOF thermal spray deposition.

Acknowledgments

The authors wish to thank the Office of Naval Research (ONR) for funding this work through grant #N00014-97-1-0560. The authors also wish to thank the Particulate Materials Characterization (PMC) Laboratory at The Pennsylvania State University where particle size measurements were performed.

References

1. W.J. Brindley: "Thermal Barrier Coatings of the Future," *J. Therm. Spray Technol.*, 1997, *6*(1), pp. 3-4.
2. D.W. Parker and G. Kutner: "HVOF-Spray Technology—Poised for Growth," *Adv. Mater. Proc.,* 1991, *4,* pp. 68-74.
3. S. Joshi and R. Sivakumar: "Particle Behavior During High Velocity Oxy-Fuel Spraying," *Surf. Coat. Technol.*, 1991, *50,* pp. 67-74.
4. P.E. Arvidsson: "Comparison of Superalloy Coatings Sprayed With Plasma and HVOF," *Powder Metall. Int.,* 1992, *24,* pp.176-79.
5. H. Kreye, S. Zimmermann, and P. Heinrich: "The Role of the Fuel Gas in the HVOF Process" in *Thermal Spraying: Current Status and Future Trends*, C.C. Berndt, ed., High Temperature Society of Japan, Osaka, 1995, pp. 393-98.
6. S.V. Joshi: "Comparison of Particle Heat-up and Acceleration During Plasma and High Velocity Oxy-Fuel Spraying," *Powder Metall. Int.*, 1992, *24,* pp. 373-77.
7. B. Kadyrov, Y. Evdokimenko, V. Kisel, and E. Kadyrov: "Calculation of the Limiting Parameters for Oxide Ceramic Particles During HVOF Spraying" in *1994 Thermal Spray Industrial Applications*, C.C. Berndt and S. Sampath, ed., ASM International, Materials Park, OH, 1994, pp. 245-50.
8. C.M. Hackett and G.S. Settles: "Turbulent Mixing of the HVOF Thermal Spray and Coating Oxidation" in *1994 Thermal Spray Industrial Applications*, C.C. Berndt and S. Sampath, ed., ASM International, Materials Park, OH, 1994, pp. 307-12.
9. V.L. Tellkamp, M.L. Lau, A. Fabel, and E.J. Lavernia: "Thermal Spraying of Nanocrystalline Inconel 718," *NanoStruct. Mater.,* 1997, *9,* pp. 489-92.
10. D.A.J. Ramm, T.W. Clyne, A.J. Sturgeon, and S. Dunkerton: "Correlations Between Spraying Conditions and Microstructure for Alumina Coatings Produced by HVOF and VPS" in *1994 Thermal Spray Industrial Applications*, C.C. Berndt and S. Sampath, ed., ASM International, Materials Park, OH, 1994, pp. 239-44.
11. A.J. Sturgeon, M.F.D. Harvey, and F.J. Blunt: "The Influence of Fuel Gas on the Microstructure and Wear Performance of Alumina Coatings Produced by the High Velocity Oxyfuel (HVOF) Thermal Spray Process," *Brit. Ceram. Proc.*, 1995, *54,* pp. 57-64.
12. Anon: "HVOF Spraying of Thermal Coatings—TWI, Abington, Cambridge, UK," *Metallurgia*, 1995, *62*(3), p. 136.
13. M.S. Cole and R. Walker: "High Temperature Erosion Properties of Thermal Barrier Coatings Produced by Acetylene Sprayed High Velocity Oxygen Fuel Process" in *Thermal Spray, Surface Engineering via Applied Research*, C.C. Berndt, ed., ASM International, Materials Park, OH, 2000, pp. 1191-99.
14. S. Stecura: "Optimization of the NiCrAlY/ZrO_2-Y_2O_3 Thermal Barrier System,"*Adv. Ceram. Mater.*, 1986, *1*(1), p. 68.
15. V.S. Stubican, J.R. Hellmann, and S.P. Ray: "Defects and Ordering in Zirconia Crystalline Solution," *Mater. Sci. Monographs*, 1982, *1,* pp. 257-61.
16. E. Underwood: "Quantitative Metallography" in *ASM Metals Handbook Metallography and Microstructures*, Vol. 9, J.R. Davis, ed., ASM International, Metals Park, OH, 1985, p. 123.
17. D.B.Cullity: *Elements of X-Ray Diffraction*, 2nd ed., Addison-Wesley, Reading, MA, 1978.
18. D. Cheng, Q. Xu, G.Trapaga, and E.J. Lavernia: "A Numerical Study of High-Velocity Oxygen Fuel Thermal Spraying Process. Part I: Gas Phase Dynamics," *Metall. Mater. Trans. A,* 2001, *32*(7), pp. 1609-20.
19. M.A. Saad: *Compressible Fluid Flow*, 2nd ed., Prentice Hall, Englewood Cliffs, NJ, 1985, p. 83.
20. H.H. Tawfik and F. Zimmerman: "Mathematical Modeling of the Gas Powder Flow in HVOF Systems," *J. Therm. Spray Technol.*, 1997, *6*(3), pp. 345-52.
21. F. Takahashi, M.D. Vangsness, M.D. Durbin, and W.J. Schmoll: "Structure of Turbulent Hydrogen Jet Diffusion Flames With or Without Swirl" in *Proceedings of the ASME Heat Transfer Division*, Vol. 317-2, R.J. Cochran, ed., American Society of Mechanical Engineers, New York, NY, 1995, pp. 183-93.
22. J.C. Lau, P.J. Morris, and M.J. Fisher: "Measurements in Subsonic and Supersonic Free Jets Using a Laser Velocimeter," *J. Fluid Mech.*, 1979, *93*(1), pp. 1-27.
23. X. Yang and S. Eidelman: "Numerical Analysis of a High-Velocity Oxygen-Fuel Thermal Spray System," *J. Thermal Spray Technol.*, 1996, *5*(2), pp. 175-84.
24. W. Kollenberg and J. Decker: "Influence of Powder-Characteristics on the Microstructure of Ceramic Plasma Spray Coatings," *Fresenius J. Anal. Chem.*, 1993, *346,* pp. 327-33.
25. B.A. Cottom and M.J. Mayo: "Fracture Toughness of Nanocrystalline ZrO_2-3mol%Y_2O_3 Determined by Vickers Indentation," *Scripta Mater.,* 1996, *34*(5), pp. 809-14.
26. R.W. Rice: *Porosity of Ceramics*, M. Dekker, New York, NY, 1998.
27. R.A. Miller, R.G. Garlick, and J.L. Smialek: "Phase Distributions in Plasma-Sprayed Zirconia-Yttria," *Ceram. Bull.* 1983, *62*(12), pp. 1355-58.
28. P.D. Harmswarth and R. Stevens: "The Microstructure of Zirconia Thermal Barrier Coatings," *Brit. Ceram. Proc.* 1989, *42,* p. 123.
29. R. Taylor, J.R. Brandon, and P. Morrell: "Microstructure, Composition and Property Relationships of Plasma-Sprayed Thermal Barrier Coatings," *Surf. Coat. Technol.*, 1992, *50,* pp. 141-49.